Second harmonic generation responses of ion pairs forming dimeric aggregates

Ramos, Tárcius N.; Castet, Frédéric; Champagne, Benoît

Published in:
The Journal of Physical Chemistry. B, Condensed matter, materials, surfaces, interfaces & biophysical

DOI:
10.1021/acs.jpcb.1c00939

Publication date:
2021

Document Version
Peer reviewed version

Second Harmonic Generation Responses of Ion Pairs Forming Dimeric Aggregates

Tárcius N. Ramos,[‡] Frédéric Castet,[†] and Benoît Champagne*[‡]

[‡] University of Namur, Theoretical Chemistry Lab, Unit of Theoretical and Structural Physical Chemistry, Namur Institute of Structured Matter, rue de Bruxelles, 61, B-5000 Namur (Belgium).

[†] Université de Bordeaux, Institut des Sciences Moléculaires, UMR 5255 CNRS, cours de la Libération 351, F-33405 Talence Cedex (France).

Abstract

A sequential approach combining molecular dynamics and density functional theory calculations has been worked out to unravel the second harmonic generation responses of anion-cation (AC) pairs when they form dimeric aggregates, where the cation is a stilbazolium derivative and the anions range from small inorganic iodide to medium-size organic *p*-toluenesulfonate. These complexes showed a strong self-aggregation behavior in molecular dynamics simulations within high-concentration conditions and formed stable dimeric aggregates, $(AC)_2$, which can adopt different structural shapes from stacked, Λ-, to head-to-head configurations. These various structures are associated with different symmetries, which are shown to modulate the second- and third-order nonlinear optical (NLO) responses. By consolidating the NLO results of this work with those previously obtained for single AC pairs [*J. Chem. Inf. Model.* **2020**, *60*, 4817–4826] we have been able to explain the experimentally-observed variations of the electrical field-induced second harmonic generation (EFISHG) responses of these complexes as a function of concentration [*ChemPhysChem* **2010**, *11*, 495–507]. Moreover, results have highlighted that i) the second-order contribution, $\mu\beta_{//}$, dominates the global EFISHG response, ii) the $\mu\beta_{//}$ responses of dimers are about half that computed for the parent AC pairs while the third-order contributions, $\gamma_{//}$, are reduced by only 10%, iii) these distinct trends are ascribed to the formation of dimers adopting mainly Λ- and head-to-head shapes, increasing the centrosymmetric character, in comparison to the monomers, a situation in which the second-order response cancels out, as well as to the influence of the dipole moment on $\mu\beta_{//}$, iv) the presence of a strong amino donor group in the cation enhances the $\mu\beta_{//}$ response by one order of magnitude and $\gamma_{//}$ by about a factor of 2, and finally, v) dimeric aggregation has similar effects on the hyper-Rayleigh scattering response, β_{HRS}, as on $\mu\beta_{//}$ while it reduces the one-dimensional character of β_{HRS}. This work constitutes a step forward for the modeling of the NLO responses of AC aggregates in solution.

1. Introduction

The experimental determination of the first (β) and second (γ), hyperpolarizabilities of molecules in solution can be carried out by probing the electrical field-induced second harmonic generation (EFISHG) response. The global EFISHG response contains second-order ($\mu\beta_{//}/3kT$, with k the Boltzmann constant and T the temperature) and third-order ($\gamma_{//}$) contributions. $\beta_{//}$ is related to the projection of the vectorial representation of β on the dipole moment (μ) while $\gamma_{//}$ is the isotropic invariant of the γ tensor. To measure the EFISHG response, an extra static electrical field is applied on the sample to create a preferential orientation of the molecules and to break the isotropicity of the medium. Due to this static electrical field, charged compounds cannot be studied by the EFISHG technique, although ionic compounds forming neutral anion-cation (A^-C^+, written in a simplified form as AC) complexes have been investigated.[1–4] The characterization of these ion pairs requires weak interactions between the ionic constituents and the solvent, to avoid the dissociation of the AC complex into solvated ions. This can be achieved by using weakly polar and aprotic solvents. Besides, large concentration dependence of the EFISHG responses has been observed in measurements,[2,5,6] which has been ascribed to the possible aggregation of these neutral AC complexes. This makes difficult the interpretation of the experimental results and, in particular, the rationalization of the EFISHG responses in terms of structure-property relationships since different AC complexes might have different degrees of aggregation.

From a theoretical point of view, the aggregation effects on the nonlinear optical (NLO) responses have been investigated for β and γ by considering aggregates in pre-established conformations such as stacked, slipped-stacked, head-to-head, and head-to-tail.[7–15] Usually, the NLO responses increase when the dimensions of the aggregate increase in the direction of the π-conjugated delocalization (as in the head-to-tail configuration) while they decrease in other cases. This can be explained in terms of simple classical electrostatic effects.[16] However, these investigations concerned neutral molecules, and, in several cases, they aimed at understanding the relationships between the responses of molecular crystals and those of their constitutive units. Recently, we have investigated the EFISHG responses of ion pairs in solution.[4,17] However, to our best knowledge, no theoretical study addressing the effects of concentration on the EFISHG responses of aggregates formed by several AC complexes has been reported yet. This is investigated here by using a computational approach combining molecular dynamic (MD) simulations and quantum mechanical (QM) calculations.

In this theoretical contribution, we investigate the EFISHG responses of a series of cationic stilbazolium derivatives in chloroform solution. These incorporate substituents ranging from H to N(n-Bu)$_2$, combined with small- to medium-size anions ranging from inorganic iodide to organic *p*-toluenesulfonate (*p*-TS). The push-pull π-conjugated character of the stilbazolium leads to sizable NLO responses, particularly in the presence of electron-donating amino substituents. The chloroform solvent avoids the dissociation of the AC complexes in the concentration range of the experimental measurements[2] allowing direct theoretical-experimental comparisons. In particular, this study targets the variations of the NLO responses when the single AC complexes aggregate into (AC)$_2$ dimers. **Figure 1** schematizes the chemical structure of such a dimer with its key geometrical parameters.

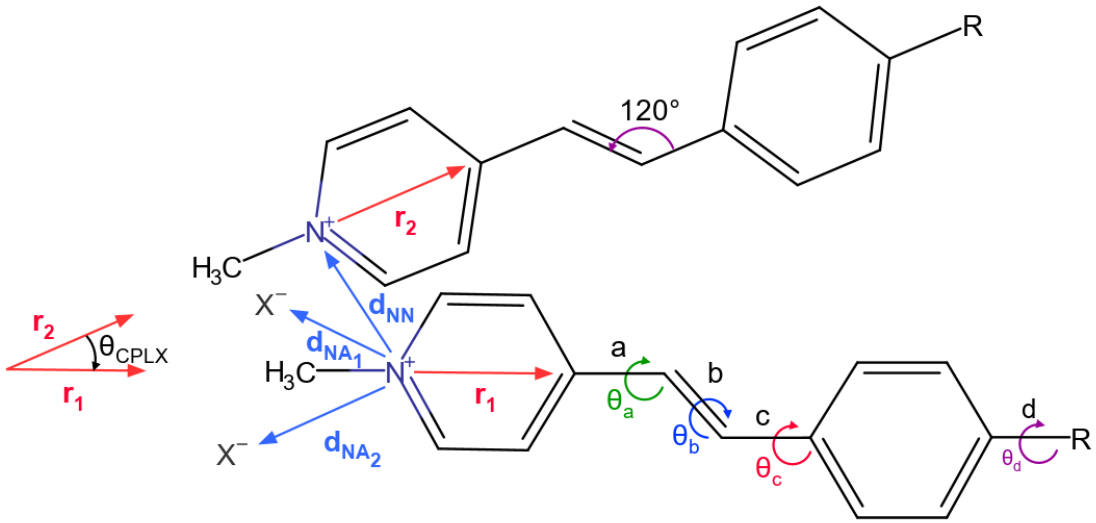

Complex:	**1** – R = H	X = I	**4.1** – R = N(n-Bu)$_2$	X = CF_3SO_3
	2 – R = tert-Bu	X = I	**4.2** – R = N(n-Bu)$_2$	X = ClO_4
	3 – R = N(Me)$_2$	X = I	**4.3** – R = N(n-Bu)$_2$	X = SCN
	4 – R = N(n-Bu)$_2$	X = I	**4.4** – R = N(n-Bu)$_2$	X = *p*-TS [a]

Figure 1. Structure of a dimer of AC complexes, with the list of R substituents and anions considered in this study. a, b, and c are the bonds used to define the bond length alternation (BLA) and θ_i $(i = a - d)$ are the torsional angles around the respective i bond (θ_d is not defined for **1** and **2**). θ_{CPLX} defines the angle formed by the directions of the pyridinium moieties of the two cations. d_{NN}, d_{NA1}, and d_{NA2} are representative interionic distances. [a] *p*-toluenesulfonate.

The computational study has been conducted in two steps. First, MD simulations were used to sample the thermodynamically accessible structures of (AC)$_2$ dimers. Then, QM methods based on the time-dependent density functional theory (TD-DFT) were employed to evaluate the NLO responses of representative configurations extracted from the MD simulations. In this second step, environment effects were accounted for by using the integral equation formalism of the polarizable continuum model[18,19] (IEFPCM). This sequential-quantum

mechanics / molecular dynamics[20,21] (S-QM/MD) approach allows describing the NLO responses of a realistic statistical set of geometrical conformations, and not only of a few pre-established ones. In addition to the EFISHG responses, we also evaluated hyper-Rayleigh scattering (HRS) responses, because they give a complementary picture of the first hyperpolarizability of the $(AC)_2$ dimers. Moreover, the linear optical responses (i.e. the UV/Vis absorption spectra) were simulated, since they help interpreting the NLO properties. Finally, statistical analyses were performed to enable comparisons with experimental results, as well as to relate the NLO responses of $(AC)_2$ dimers to their electronic and geometrical properties.

The paper is organized as follows. In Section 2 we describe key elements of molecular nonlinear optics and the computational methods employed in the S-QM/MD approach. The structural features of $(AC)_2$ dimers, their linear and nonlinear optical responses, as well as structure-property analyses, and comparison with experimental data are reported in Section 3. The main conclusions are drawn in Section 4.

2. Methods

2.1. Nonlinear Optical Properties

At the molecular scale, the linear and nonlinear optical properties are defined by the expansion of the induced electric dipole moment ($\Delta\vec{\mu}$) in terms of external electric fields ($\vec{E}$) oscillating at ω angular frequencies. Eq. (1) defines the polarizability (α), the first (β), and the second (γ) hyperpolarizability tensor elements, adopting the T convention:

$$\begin{aligned}\Delta\mu_i(-\omega_\sigma) = & \sum_j^{x,y,z} \alpha_{ij}(-\omega_\sigma;\omega_1)E_j(\omega_1) \\ & + \frac{1}{2!}\sum_{j,k}^{x,y,z} \beta_{ijk}(-\omega_\sigma;\omega_1,\omega_2)E_j(\omega_1)E_k(\omega_2) \\ & + \frac{1}{3!}\sum_{j,k,l}^{x,y,z} \gamma_{ijkl}(-\omega_\sigma;\omega_1,\omega_2,\omega_3)E_j(\omega_1)E_k(\omega_2)E_l(\omega_3) \\ & + \cdots\end{aligned} \quad (1)$$

where $\omega_\sigma = \sum_n \omega_n$ and the lower-case indices define the molecular axes coordinates (x, y, z).[22] The EFISHG setup probes the second harmonic generation (SHG) response of solutions, with $\omega_3 = 0$ and $\omega_1 = \omega_2 = \omega$. It contains both a β and a γ contribution:[23]

$$\gamma_{EFISHG} = \gamma_{//}(-2\omega;\omega,\omega,0) + \frac{\mu\beta_{//}(-2\omega;\omega,\omega)}{3kT} = \frac{\left[\mu\beta_{//}(-2\omega;\omega,\omega)\right]_{eff}}{3\mathrm{kT}} \quad (2)$$

where μ is the norm of the ground state dipole moment and $3kT = 2.833 \times 10^{-3}$ a.u. at room temperature. As evidenced from Eq. (2), measurements should be performed at different temperatures to separate the second- and third-order responses. However, this is rarely done because the range of accessible temperatures is narrow and because the $\gamma_{//}$ contribution is assumed to be negligible, which is substantiated for compounds with large μ and β values.[24,25] Therefore, the effective $\left[\mu\beta_{//}(-2\omega;\omega,\omega)\right]_{eff}$ response is commonly employed for comparing molecular responses as well as for interpreting experimental data in light of quantum chemical results. Formally, the $\beta_{//}$ and $\gamma_{//}$ values are obtained by combining the tensor elements as follows. $\beta_{//}$ is related to the projection of the vectorial representation of the β tensor on the dipole moment:

$$\beta_{//}(-2\omega;\omega,\omega) = \beta_{//} = \frac{3}{5\mu}\,\vec{\mu}\cdot\vec{\beta} \quad (3)$$

where the β vector components read:

$$\beta_i = \frac{1}{3}\sum_{j}^{x,y,z}(\beta_{ijj} + \beta_{jij} + \beta_{jji}) \quad (4)$$

On the other hand, $\gamma_{//}$ corresponds to the isotropic invariant of the γ tensor:

$$\gamma_{//}(-2\omega;\omega,\omega,0) = \gamma_{//} = \frac{1}{15}\sum_{i,j}^{x,y,z}(2\gamma_{iijj} + \gamma_{ijji}) \quad (5)$$

The relative amplitudes of the second- and third-order contributions to the global EFISHG response can be analyzed using the $R_{3/2}$ ratio:

$$R_{3/2} = \gamma_{//} \times \frac{3kT}{\mu\beta_{//}} \quad (6)$$

In the HRS technique, the sampled quantity is solely the second harmonic generation β tensor.[26] Typical HRS experiments collect the vertically-polarized scattered light at an angle of 90° with respect to the incident light direction. The $\beta^2_{HRS}(-2\omega;\omega,\omega)$ quantity is related to the scattered light intensity. It is given by the sum of two terms, $\langle\beta^2_{ZZZ}\rangle$ and $\langle\beta^2_{ZXX}\rangle$, obtained

by performing an averaging over all possible molecular orientations (assuming an isotropic distribution), which correspond to the contributions of vertically- and horizontally-polarized incident light, respectively:

$$\beta_{HRS}(-2\omega;\omega,\omega) = \beta_{HRS} = \sqrt{\langle\beta_{ZZZ}^2\rangle + \langle\beta_{ZXX}^2\rangle} \quad (7)$$

The relations between these quantities defined in the laboratory frame (upper-case indices) and the β tensor components defined in the molecular coordinates system (lower-case indices) read:

$$\langle\beta_{ZZZ}^2\rangle = \frac{1}{105}\sum_{ijk}^{x,y,z}\left[2\beta_{ijk}^2 + \beta_{ijj}\beta_{ikk} + 4\left(\beta_{iij}\beta_{jkk} + \beta_{iij}\beta_{kkj} + \beta_{ijk}\beta_{jik}\right)\right] \quad (8)$$

$$\langle\beta_{ZXX}^2\rangle = \frac{1}{105}\sum_{ijk}^{x,y,z}\left[6\beta_{ijk}^2 + 3\beta_{ijj}\beta_{ikk} - 2\left(\beta_{iij}\beta_{jkk} + \beta_{iij}\beta_{kkj} + \beta_{ijk}\beta_{jik}\right)\right] \quad (9)$$

From their analysis, and more precisely from the Depolarization Ratio (DR)

$$DR = \frac{\langle\beta_{ZZZ}^2\rangle}{\langle\beta_{ZXX}^2\rangle} \quad (10)$$

information can be deduced on the shape of the harmonophore, *i.e.* the part of the probed molecular system that scatters the SHG signal. So, DR ranges from 1.5 to 9 for a perfect octupolar and dipolar shape, respectively. In addition, when the β tensor is dominated by one single diagonal element, oriented along the charge transfer axis (usually the dipole moment axis for neutral species), DR = 5, and the system is referred to as one-dimensional (1-D).

2.2. Molecular Dynamics Simulations

The NLO responses of stilbazolium AC complexes in chloroform solution depend on the concentration, and such dependence is directly related to the formation of AC aggregates. The self-aggregation process of AC pairs was investigated by using MD simulations assuming highly-concentrated media. Simulations were performed in a cubic box of 120 Å edge in the NPT ensemble under Standard Ambient Temperature and Pressure (T = 298.15 K and P = 1 atm) and using periodic boundary conditions. The initial boxes were filled up using smaller chloroform boxes, containing 250 chloroform molecules each and previously thermalized. Then, 15 AC pairs were inserted randomly into the box by imposing two

constraints: i) the minimum distance between two different AC complexes is larger than 20 Å, and ii) the distance between a given AC complex and the border of the box is also larger than 20 Å. These two constraints prevent from forming artificial aggregates at the beginning of the simulation, including those formed by an AC complex with any periodic image. From these starting samples, a thermalization step of 3 ns was first conducted, along which the position of each AC pair was kept fixed to allow the stabilization of solute-solvent and solvent-solvent interactions. Then, MD simulations of 10 ns were run without any constraints to allow the self-aggregation process.

As a consequence of the high-concentration conditions assumed here for practical means, these MD runs produced aggregates of various sizes. The present study focuses on dimers, $(AC)_2$, the smallest and first thermodynamically and kinetically accessible aggregates. Thus, several structures of these $(AC)_2$ aggregates were extracted from the MD trajectories and used as starting points for studying their dynamics. These new set of MD simulations were performed on cubic boxes of 95 Å edge containing the selected $(AC)_2$ dimers, which were filled up using the previously thermalized small chloroform boxes. After an equilibration stage of 5 ns without imposing any restriction on the atomic motions, a production run of 25 ns was performed, along which 100 geometrical configurations (equally spaced by 250 ps) of the $(AC)_2$ dimers were extracted in view of subsequent calculations of the NLO responses.

All MD simulations were performed by employing the leapfrog solver.[27] The Berendsen barostat[28] and the velocity rescaling thermostat[29] were coupled every 1 ps and 0.1 ps, respectively. The short-range nonbonding interactions were defined inside a cutoff radius of 17 Å and the long-range electrostatic corrections were accounted for by the smooth Particle-Mesh Ewald method.[30] The All-Atom Optimized Potentials for Liquid Simulations[31] (OPLS-AA) force field was employed for both the chloroform molecules and the AC complexes. The force fields parameters of the AC complexes are the same as in our recent investigation.[17] The equilibrium bond lengths, valence angles, and torsional parameters were refined to fit the equilibrium geometries obtained from DFT calculations at the IEFPCM(chloroform)/ωB97X-D/aug-cc-pVDZ level (the aug-cc-pVDZ-PP basis set including pseudo-potentials was used for iodine). The atomic charges were obtained using the CHELPG electrostatic mapping.[32] The chloroform OPLS-AA parameters were obtained from Ref. 33. MD simulations were performed using the Gromacs software.[34,35]

2.3. Calculations of Optical Properties

The linear and nonlinear optical responses of the $(AC)_2$ dimers extracted from the MD runs were computed using the TD-DFT method with the M06-2X[36] exchange-correlation functional and the 6-311+G(d) basis set. A pseudo-potential aug-cc-pVDZ-PP basis set was employed for the iodine atom. The M06-2X exchange-correlation functional was selected due to its good balance between DFT and Hartree-Fock exchange contributions.[37] This level of calculation is the same as in our previous study performed on single ion pairs (AC),[17] which enables direct comparisons. In this former study, we demonstrated that using larger basis sets such as 6-311+G(d,p) and aug-cc-pVDZ for all atoms types, except iodine, impacts by less than 3% the NLO responses. This good compromise between accuracy and calculation costs motivated our specific choice of the 6-311+G(d) basis set for the present study of larger complexes. Solute-solvent interactions were described in all TD-DFT calculations by using IEFPCM.[18,19] Although explicit solvation models are more realistic, the inclusion of explicit chloroform molecules should induce little changes due to the weak solute-solvent interactions, and the small HRS response of liquid chloroform[38] (~20 a.u.) compared to AC complexes (~2-13 10^3 a.u.). The dynamic NLO responses were calculated using a 1907 nm wavelength as used in the experimental measurements. Vertical transition energies and oscillator strengths were evaluated at the same level of approximation, in order to help to rationalize the NLO responses. In particular, the determination of excitation energies allows assessing whether the dynamic NLO responses are impacted by electronic resonance effects. All QM calculations were performed with the Gaussian16[39] software.

As mentioned above, 100 geometrical configurations of the $(AC)_2$ dimers extracted every 250 ps of the MD production runs were considered for calculating the NLO properties. To address the quality of their convergence, 100 additional structures were considered for $(AC)_2$ dimers **1** and **4.2**, resulting in a statistical sampling including 200 snapshots equally-spaced by 125 ps. These complexes have been selected because they present the smallest (**1**) and the largest (**4.2**) experimental EFISHG responses and comprise weak (**1**) and strong (**4.2**) donor groups. Moreover, owing to the size of the $(AC)_2$ dimers and the need of performing a large number of calculations on statistical sets of configurations, we checked the effect of reducing the tightness of the grid used for numerical integrations in the calculation of the NLO responses. An integration grid is defined by the number of radial shells (RS) and by the number of angular points per shell (AS) as (RS, AS). Two sets of grids were used for this purpose on 10 randomly selected configurations of **1** and **4.2**. Two couples of integration grids implemented in Gaussian 16 were employed for the SCF (Self-Consistent Field) and

CPHF (Coupled-Perturbed Hartree-Fock) calculation steps: (i) “ultrafine” (99, 590) and “fine” (75, 302) versus (ii) “fine” and “coarse” (35, 110).

3. Results and Discussion

3.1. Structure of $(AC)_2$ dimeric aggregates

Visual analyses of the MD trajectories showed that the $(AC)_2$ dimers are linked by the interactions between their anion and the methylpyridinium groups. The dimers are stable during the whole MD simulation time and present stacked, head-to-head, and Λ-shape configurations with larger probability for the latter while no head-to-tail configuration was observed. $(AC)_2$ structures extracted from the self-aggregation simulations and used as starting configurations for the MD simulations are displayed in **Figure S1**. As defined in **Figure 1**, several parameters were considered to analyze their geometrical features: i) d_{NN}, the distance between the nitrogen atoms of the two methylpyridinium groups, ii) d_{NA}, the distance between the nitrogen atom of the methylpyridinium group and the atom A of the anion (where A is I, S, Cl, C, and S for I^-, $CF_3SO_3^-$, ClO_4^-, SCN^-, and *p*-TS^-, respectively), and iii) θ_{CPLX}, the angle formed by the direction of the pyridinium moieties of the chromophores, so that if $\theta_{CPLX} = 0°$ the dimers are in perfect stacked conformation while if $\theta_{CPLX} = 180°$ they adopt a head-to-head shape. Λ-shapes correspond to intermediate θ_{CPLX} values.

Statistical distributions of d_{NN} values shown in the left-hand side of **Figure 2** exhibit one asymmetrical peak centered around 5.2-5.7 Å, except for **4.4** implying a *p*-TS anion, for which the maximum of the distribution is markedly shifted to lower values and centered at 4.27 Å. Due to these asymmetrical shapes, the distributions were fitted with a combination of two Gaussian functions. The distribution maxima values are collected in **Table 1** and the Gaussian functions characteristics are given in the insets of **Figure 2**. The maxima of the d_{NN} distributions are observed at larger values for **4**, **4.2**, and **4.3** indicating a less compact aggregation than for the other $(AC)_2$ dimers. At the same time, for these complexes, the center of the second Gaussian function is located around 7.0 Å with a standard deviation of ~1.1 Å. The distributions of d_{NA} distances (right-hand side of **Figure 2**) display two peaks for $(AC)_2$ dimers involving iodide anions (**1**-**4**) and a single peak for the other complexes (**4.1**-**4.4**). The distributions were fitted with a combination of three Gaussian functions, with results presented in **Table 1** and on insets of **Figure 2**.

Table 1. d_{NN} and d_{NA} values (Å) corresponding to maxima of the statistical distributions for the different $(AC)_2$ dimers shown in **Figure 2**, as well as average θ_{CPLX} and their standard deviations (degrees) from the distributions shown in **Figure 3**.[a]

Complex	d_{NN}	d_{NA}	θ_{CPLX}
1	5.43	4.30/6.09 (4.27) [4.21]	95 ± 44
2	5.41	4.30/6.10 (4.28) [4.21]	109 ± 42
3	5.22	4.36 (4.33) [4.26]	107 ± 42
4	5.55	4.37/6.16 (4.36) [4.26]	93 ± 42
4.1	5.26	4.62 (4.38) [4.36]	103 ± 47
4.2	5.74	4.57 (4.40) [4.36]	105 ± 39
4.3	5.74	4.31 (4.16) [4.07]	101 ± 45
4.4	4.27	4.63 (4.28) [4.30]	32 ± 28

[a] Average d_{NA} values for the AC complexes (in parentheses) and maxima of their statistical distributions (in brackets) (Ref. 17).

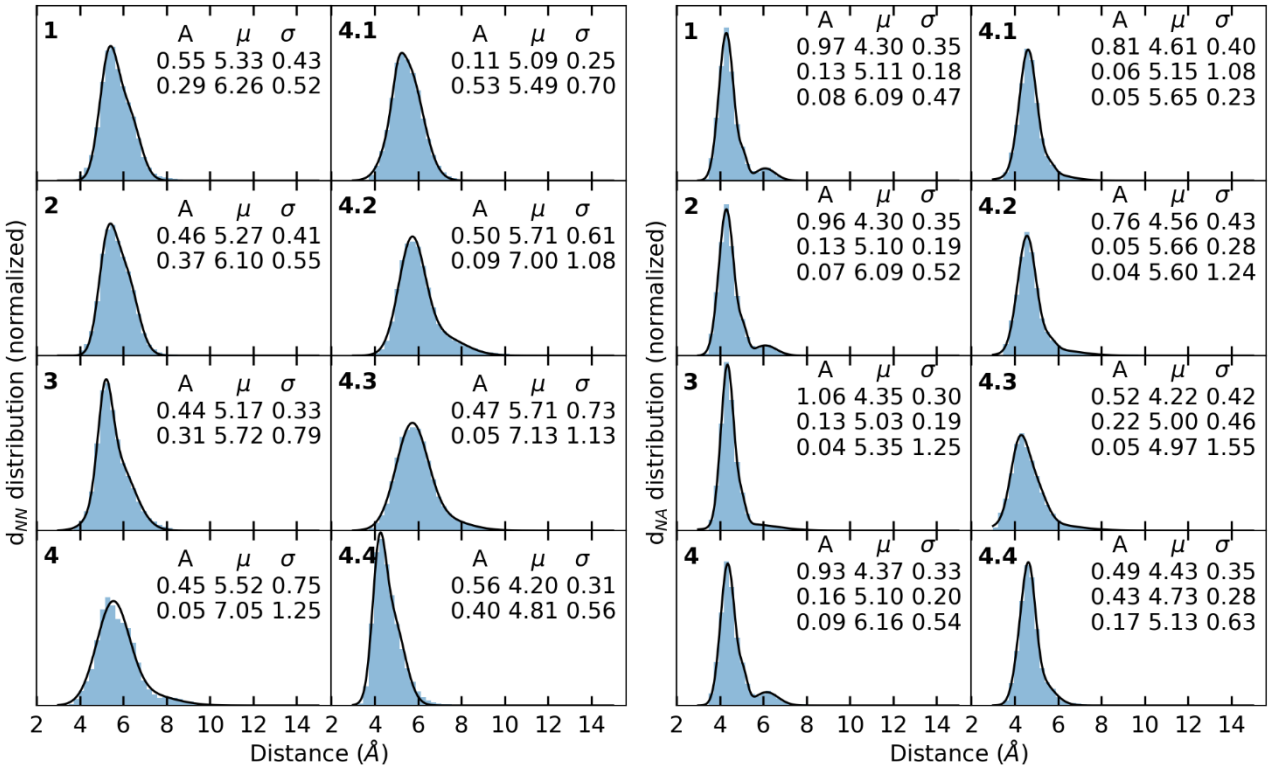

Figure 2. Distributions of the d_{NN} and d_{NA} distances for $(AC)_2$ dimers issued from MD trajectories. The black line is the result of fitting the data with a combination of Gaussian functions. Their characteristics are given in the insets (A is the amplitude, μ is the center, and σ is the standard deviation of each function). The maxima are reported in **Table 1**.

The d_{NA} dominant peaks for **1**-**4** are centered around 4.3 Å, a value very similar though about 0.1 Å larger than that of the AC complexes. Then a second distinguishable peak appears around 6.1 Å. It is associated with structures in which one of the anions interacts with the two cations, while the other anion mainly interacts with only one cation. On the other hand, for **4.1**-**4.4**, the d_{NA} distribution maxima are 0.21-0.33 Å larger than for the corresponding AC complex. These larger d_{NA} values for **4.1**-**4.4** are related to the size of the

anion, larger anions leading to larger d_{NA} values. The smaller d_{NN} value, the slightly larger d_{NA} value, combined with a small average θ_{CPLX} (32°) value as observed for **4.4** suggests the predominance of stacked forms.

As illustrated in **Figure 3**, the distributions of the θ_{CPLX} angles are very broad and show slightly larger probabilities for angles around 150°. Exceptions occur for **4.1** and mostly for **4.4**, which display a prominent structure centered around 15°, which indicates that this complex adopts preferentially stacked configurations. The relationships between θ_{CPLX} values and the NLO responses of the $(AC)_2$ dimers will be discussed hereafter. The amplitude of the bond length alternation along the vinylic bridge of the stilbazolium cations (BLA = [(a+c)/2 - b)], **Figure 1**) was also sampled along the MD simulations. This parameter plays an important role on the NLO responses since it is directly related to the degree of π-electron conjugation within the structures. As reported in **Table 2**, average BLA values of $(AC)_2$ dimers are similar to those of the parent AC complexes, evidencing that the intramolecular charge transfer is not modified by the aggregation process. These results also confirm for dimeric complexes that dialkylamino donor groups in the cations of **3** and **4**-**4.4** give rise to smaller BLA values than the weaker donor substituents implied in **1** and **2**.

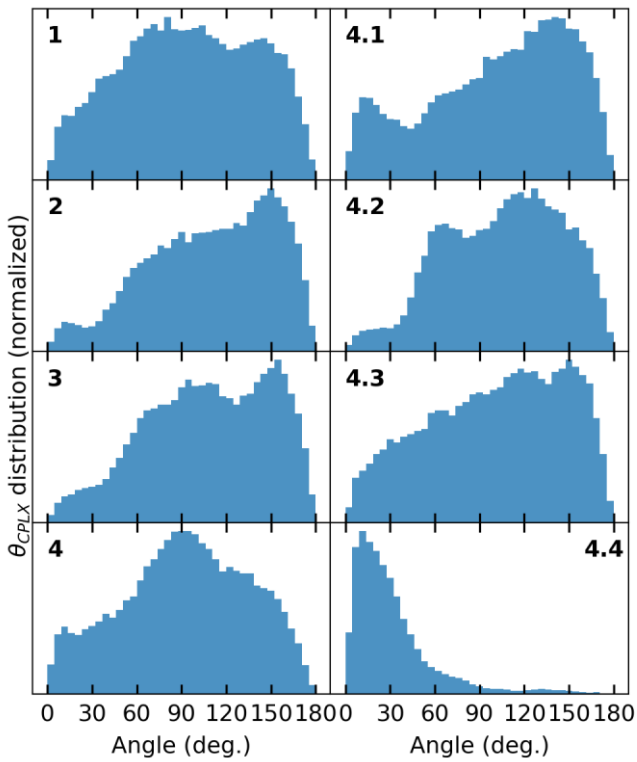

Figure 3. Normalized distribution of θ_{CPLX} values in $(AC)_2$ dimers issued from MD trajectories.

Table 2. Average bond length alternation (BLA) and standard deviations (Å) for AC and $(AC)_2$ issued from MD trajectories.[a]

Complex	State of Aggregation	BLA	Complex	State of Aggregation	BLA
1	AC	0.116 ± 0.030	**4.1**	AC	0.094 ± 0.030
	$(AC)_2$	0.116 ± 0.030		$(AC)_2$	0.094 ± 0.030
2	AC	0.115 ± 0.029	**4.2**	AC	0.098 ± 0.030
	$(AC)_2$	0.115 ± 0.030		$(AC)_2$	0.098 ± 0.030
3	AC	0.097 ± 0.030	**4.3**	AC	0.098 ± 0.030
	$(AC)_2$	0.097 ± 0.030		$(AC)_2$	0.098 ± 0.030
4	AC	0.094 ± 0.030	**4.4**	AC	0.101 ± 0.030
	$(AC)_2$	0.094 ± 0.030		$(AC)_2$	0.101 ± 0.030

[a] Values for the AC complexes are taken from Ref. 17.

Finally, the intramolecular charge transfer also depends on the torsion angles θ_{a-c} around the single bonds involved in the BLA definition, as well as on the orientation of the R substituent with respect to the terminal phenyl ring (θ_d, **Figure 1**), more planar systems giving rise to stronger push-pull effects. As for the BLA, the distributions of these four angles for the different types of $(AC)_2$ dimers (**Figure 4**) have similar shapes to those obtained for their parent AC complexes. The distributions of θ_b show one sharp peak around 180°, revealing that only trans configurations are accessible along the MD trajectories. The peaks centered at 0° and 180° for θ_a and θ_c demonstrate that the structures are planar. Yet, the distributions are broader than for θ_b. These are even broader for θ_d, associated with the rotation of the di-alkyl-amino substituent, highlighting the presence of a large number of configurations with lesser π-electron conjugation.

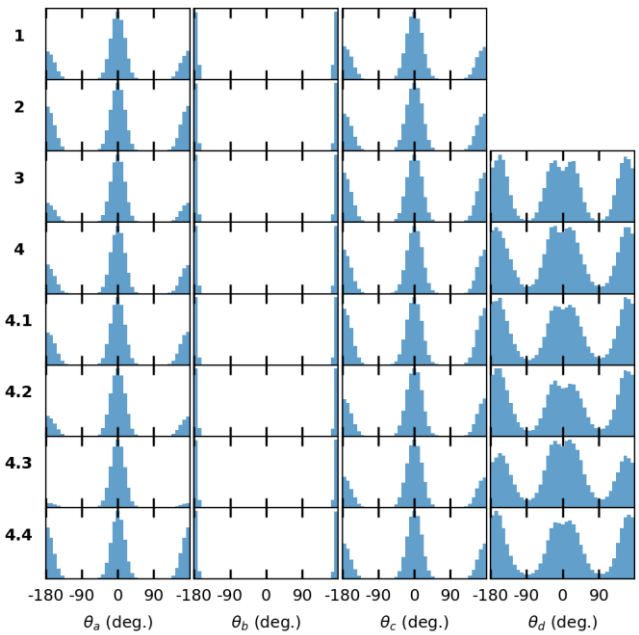

Figure 4. Distributions of the θ_{a-d} torsional angles in $(AC)_2$ dimers issued from MD trajectories.

3.2. EFISHG responses

In the following sections, the NLO responses of any $(AC)_2$ dimer have been divided by 2 in comparison to the raw computed values, and thus they correspond to the average value per AC ion pair within the aggregate. Owing to the large number of geometrical configurations considered in NLO calculations (1000 in total), preliminary calculations were performed in order to define the best compromise between accuracy and computational needs. The effect of the integration grid mesh on the EFISHG properties was first addressed for a set of 10 randomly selected configurations of **1** and **4.2** dimers. As shown in **Table S1**, reducing the density of points from “ultrafine” to “fine” in the SCF step and from “fine” to “coarse” in the CPHF step induces variations smaller than 4% of the NLO responses, while the computational time is substantially reduced by 10-34%. We also note that the standard deviations of the NLO responses of the sampled configurations are much larger than these differences (vide infra), ensuring the reliability of employing the coarser integration grids for this study.

Subsequently, cumulative averages of the NLO responses of complexes **1** and **4.2** forming dimeric aggregates, as well as their respective standard deviations, were obtained by considering 100 and 200 configurations sampled every 250 and 125 ps of the MD trajectories, respectively. As shown in **Figure S2**, the averages and standard deviations considering 100 and 200 configurations are in good agreement with each other. Although the convergence of cumulative averages presents slightly different behaviors, these results demonstrate that all properties reach convergence using the smaller sampling set. In addition, the cumulative averages and standard deviations values achieved for all complexes within 100 configurations are presented in **Figure S3** and **S4**. A similar convergence of the average values for all compounds further supports the employment of 100 configurations. Therefore, all results reported in the following were obtained on the basis of 100 configurations.

Numerical data related to the EFISHG response are presented in **Table 3**. The second-order EFISHG $\mu\beta_{//}$ responses of **1** and **2** are about one order of magnitude smaller than those obtained for **3** and **4**, owing to the presence of strong amino donor groups on the terminal phenyl ring in the latter. The same trend is observed for the $\beta_{//}$ values, while the dipole moments μ are multiplied by about 2. As discussed above, MD simulations provide different shapes for the $(AC)_2$ dimers, going from stacked to head-to-head configurations. Due to this wide range of possible geometrical arrangements, the standard deviations of $\mu\beta_{//}$ are large and range from 80% (for **4**) to 133% (for **1**) of their respective averages. **4.4** stands as an

exception with the smallest relative standard deviation (36%), consistently with the more peaked distribution of the θ_{CPLX} angle. Although the $(AC)_2$ dimers of **4** to **4.3** involve anions of different nature, they little impact the $\mu\beta_{//}$ responses, which amount to ~95 10^3 a.u. On the other hand, **4.4** exhibits larger values for $\beta_{//}$ (18.6 10^3 a.u.) and μ (8.62 a.u.), which, when combined with the smallest $\theta_{(\mu,\beta)}$ angle ($\approx 18°$), lead to the largest $\mu\beta_{//}$ response (164 10^3 a.u.). This effect is related to the predominance of stacked dimeric aggregates, as well as to the more efficient intramolecular charge transfer induced by the presence of N(n-Bu)$_2$ substituents.

Except for **4.4**, the $\mu\beta_{//}$ values of $(AC)_2$ dimers are reduced by ~50% in comparison to those obtained in the case of the parent AC complexes. This behavior can be rationalized by analyzing the independent variations of the μ, $\beta_{//}$ and $\theta_{(\mu,\beta)}$ averages. From AC to $(AC)_2$, the dipole moment μ decreases from 30% (**4.2**) to 68% (**2**), dictating in a good extent the behavior of $\mu\beta_{//}$. With the exception of **1** the $R_{D/M}$ (= [$(AC)_2$ / 2 (AC)]) ratios for $\beta_{//}$ are also smaller than one and range from 0.58 (**4.3**) to 0.86 (**2**). In parallel, the $\theta_{(\mu,\beta)}$ values are also reduced in comparison to the AC complexes, conversely favoring an increase of $\mu\beta_{//}$. This lowering of the $\theta_{(\mu,\beta)}$ angle is quite systematic and amounts to 20° in the **1**-**4** series, while the difference gets smaller when replacing the iodide with other types of anions in complexes **4.1**-**4.3**. The only exception to this general reduction by half of $\mu\beta_{//}$ is again found for **4.4**, for which $\mu\beta_{//}$ is reduced by only 10% in comparison to the value computed for the corresponding monomer. This is mainly due to the slight increase (+7%) of the dipole moment, whereas μ significantly decreases in all other $(AC)_2$ aggregates.

On the other hand, the third-order EFISHG contribution ($\gamma_{//}$) is much less impacted by aggregation effects, with a general reduction of less than 10% in comparison to the values obtained for single AC complexes. Exceptions to this trend are observed for **2**, for which $\gamma_{//}$ slightly increases by 7%, and again for **4.4**, which conversely shows a significant 28% decrease.

Despite the larger decrease of $\mu\beta_{//}$ compared to $\gamma_{//}$, the second-order contributions remain larger than the third-order ones in $(AC)_2$ dimers. This is first evidenced by the $R_{3/2}$ ratios, whose average values vary from 0.04 (**4.1**) to 0.5 (**2**), though for **1** and **3** they are as large as 1.8 and 1.4, respectively. Note that huge standard deviations on the $R_{3/2}$ values are obtained for **1**, **3**, and **4.3**, which originate from a few outlier points for which $\mu\beta_{//} \rightarrow 0$ because $\theta_{(\mu,\beta)} \approx 90°$, leading to a negative sign of $R_{3/2}$ for **4.3**. These outliers are more

easily accessible in $(AC)_2$ dimers than in the parent AC monomers due to their higher structural complexity and flexibility.

The impact of these outliers can be damped by considering an alternative definition of the $R_{3/2}$ ratio, $\tilde{R}_{3/2} = \bar{\gamma}_{//} \times (3kT/\overline{\mu\beta}_{//})$, where the bar represents the average value. These more representative ratios are all smaller than one, with the largest values (0.29 and 0.25) found for **1** and **2**, respectively. The smallest values (comprised between 0.03-0.09) are obtained for $(AC)_2$ dimers in which the cationic chromophores bear amino substituents, which confirms that the third-order EFISHG contribution can be considered as negligible compared to the second-order term for π-conjugated systems with strong push-pull character.

3.3. HRS responses

The HRS data reported in **Table 3** show that the smallest β_{HRS} values are obtained for **1** and **2**, again due to the absence of strong electron-donating amino groups. This trend is similar to that observed for the EFISHG responses, although the enhancement induced by the N(*n*-Bu)$_2$ substituents on β_{HRS} is smaller than that caused on $\mu\beta_{//}$ values. Overall, the average β_{HRS} values of $(AC)_2$ dimers are reduced by 31-44% compared to the corresponding parent AC complex, with once again the smallest variation obtained for **4.4**. The relative standard deviations of β_{HRS} values range between 17% (**4.4**) and 33% (**4.2**). They are much smaller than relative standard deviations calculated for $\mu\beta_{//}$, evidencing the weaker dependence of the HRS signal on structural fluctuations. The symmetry of the harmonophores can be further assessed by analyzing the depolarization ratios. For $(AC)_2$ dimers, average DR values range from 3.7 to 5.3, with standard deviations around 1.3. DR values span therefore a broad range of values, with minima lying between 1.8-2.5 and maxima comprised between 6.3-6.8. In comparison, the DR distributions calculated for single AC complexes of **3**-**4.4** are much sharper and closer to the typical case of 1-D-like harmonophores, with values equal to 4.7 ± 0.1. Therefore, the NLO responses of $(AC)_2$ dimers, owing to their higher structural flexibility, do not present any marked symmetry character and fluctuate between the dipolar and octupolar limits. Still, within the series, **4.4** exhibits the largest average DR value together with the smallest standard deviation (5.34 ± 0.70), consistently with the strong push-pull character and the preferential parallel stacking of the π-conjugated cationic species.

Table 3. EFISHG and HRS responses of $(AC)_2$ dimers and dimer/monomer ratios ($R_{D/M}$, in parentheses) calculated at 1907 nm[a,b].

	1	**2**	**3**	**4**
$\mu\beta_{//}$	6 ± 8 (0.49)	12 ± 13 (0.43)	77 ± 70 (0.47)	94 ± 75 (0.5)
$\beta_{//}$	1.6 ± 1.6 (1.12)	2.7 ± 2.3 (0.86)	11.7 ± 7.1 (0.7)	14.5 ± 7.2 (0.8)
μ	3.65 ± 1.99 (0.43)	3.65 ± 2.12 (0.42)	5.65 ± 2.83 (0.59)	6.20 ± 3.54 (0.63)
$\theta_{(\mu,\beta)}$	53.8 ± 37.3	46.8 ± 33.5	30.9 ± 28.5	30.9 ± 25.2
β_{HRS}	2.2 ± 0.5 (0.57)	3.1 ± 1.0 (0.56)	10.6 ± 3.2 (0.58)	12.8 ± 3.2 (0.61)
DR	3.73 ± 1.16	3.65 ± 1.29	4.09 ± 1.31	4.42 ± 1.31
$\mu\beta_{//}/3kT$	2.3 ± 2.9 (0.49)	4.3 ± 4.7 (0.43)	27.3 ± 24.7 (0.47)	33.3 ± 26.5 (0.5)
$\gamma_{//}$	0.66 ± 0.09 (0.91)	1.0 ± 0.7 (1.07)	2.5 ± 0.3 (0.96)	2.8 ± 0.5 (0.93)
γ_{EFISHG}	2.9 ± 2.9 (0.55)	5.3 ± 4.7 (0.49)	29.8 ± 24.6 (0.49)	36.1 ± 26.4 (0.52)
$R_{3/2}$	1.8 ± 12.0	0.5 ± 2.6	1.4 ± 13.8	0.2 ± 0.3
$\tilde{R}_{3/2}$	0.289	0.245	0.091	0.085
$\left[\mu\beta_{//}\right]_{eff}^{X}$ [c]	76 ± 74 (0.55)	137 ± 121 (0.49)	773 ± 638 (0.49)	936 ± 683 (0.52)
$\left[\mu\beta_{//}\right]_{eff}^{X}$ (exp) [d]	800; 300; 170	810; 600; 205	1700; 1000; 1000	1900; 1400; 1090
	4.1	**4.2**	**4.3**	**4.4**
$\mu\beta_{//}$	92 ± 81 (0.47)	96 ± 99 (0.51)	96 ± 87 (0.45)	164 ± 58 (0.91)
$\beta_{//}$	13.7 ± 7.8 (0.68)	12.0 ± 9.3 (0.65)	12.3 ± 8.5 (0.58)	18.6 ± 4.2 (0.85)
μ	5.49 ± 2.98 (0.58)	6.76 ± 4.06 (0.7)	6.46 ± 3.39 (0.66)	8.62 ± 1.87 (1.07)
$\theta_{(\mu,\beta)}$	30.5 ± 31.0	40.7 ± 38.3	37.3 ± 31.6	17.3 ± 11.9
β_{HRS}	11.8 ± 3.7 (0.57)	11.7 ± 3.8 (0.56)	11.8 ± 3.8 (0.57)	13.4 ± 2.3 (0.69)
DR	4.09 ± 1.28	4.29 ± 1.41	4.21 ± 1.34	5.34 ± 0.70
$\mu\beta_{//}/3kT$	32.5 ± 28.5 (0.47)	33.7 ± 35.1 (0.51)	33.7 ± 30.6 (0.45)	57.8 ± 20.3 (0.91)
$\gamma_{//}$	2.5 ± 0.5 (0.92)	2.5 ± 0.4 (0.93)	2.6 ± 0.5 (0.9)	1.9 ± 0.3 (0.72)
γ_{EFISHG}	35.0 ± 28.3 (0.48)	36.3 ± 35.0 (0.53)	36.4 ± 30.5 (0.46)	59.7 ± 20.3 (0.9)
$R_{3/2}$	0.04 ± 0.63	0.3 ± 4.1	-0.8 ± 12.3	0.05 ± 0.06
$\tilde{R}_{3/2}$	0.077	0.075	0.078	0.033
$\left[\mu\beta_{//}\right]_{eff}^{X}$ [c]	908 ± 734 (0.48)	940 ± 906 (0.53)	942 ± 790 (0.46)	1547 ± 526 (0.9)
$\left[\mu\beta_{//}\right]_{eff}^{X}$ (exp) [d]	1150; 710; 225	1950; 1200; 250	1800; 1800; 1790	1150; 780; 690

[a] Averages and standard deviations for $\mu\beta_{//}$ (10^3 a.u.), $\beta_{//}$ (10^3 a.u.), μ (a.u.), $\theta_{(\mu,\beta)}$ (deg.), β_{HRS} (10^3 a.u.), depolarization ratios (DR), $\mu\beta_{//}/3kT$ (10^6 a.u.), $\gamma_{//}$ (10^6 a.u.), γ_{EFISHG} (10^6 a.u.), and $\left[\mu\beta_{//}\right]_{eff}^{X}$ (10^{-48} esu). $R_{3/2} = \gamma_{//} \times (3kT/\mu\beta_{//})$ and $\tilde{R}_{3/2} = \bar{\gamma}_{//} \times (3kT/\overline{\mu\beta}_{//})$ (where bars stand for average values).

[b] $R_{D/M}$ = [$(AC)_2$ / 2 (AC)] ratios, calculated using monomer values from Ref. 17

[c] Following Ref. 2, $\left[\mu\beta_{//}\right]_{eff}^{X}$ values are given (in 10^{-48} esu) within the X convention, with $\left[\mu\beta_{//}\right]_{eff}^{X} = \frac{5}{12}\left[\mu\beta_{//}\right]_{eff}^{T}$.

[d] Experimental data measured at concentrations of 1 10^{-4}, 5 10^{-4}, and 1 10^{-3} M, respectively.[2]

Figure 5 further illustrates the complexity of the relationships between the structure of the aggregates and the symmetry of their HRS responses, as it reports the Unit Sphere Representations of the first hyperpolarizability tensors for particular $(AC)_2$ dimers extracted from MD trajectories among those having the strongest 1-D character. Complexes **4**, **4.3**, and **4.4** exhibit the largest induced dipole moments consistently to their stacked structures. **1**, **2**, **4.1**, and **4.2** display Λ-shape structures with θ_{CPLX} values of 36°, 90°, 96°, and 87°, respectively. The largest induced dipoles in **1** are oriented parallel to the median of the cation dimer, while their direction in **2** and **4.1** correspond to the main inertial axis of one of the cations. On the other hand, in **4.2** they point along the long axes of both cations. This behavior is ascribed to the relative position of the cations and anions, which allows comparable contributions from both AC complexes. The smallest HRS response is observed for **3**, which displays a head-to-head configuration.

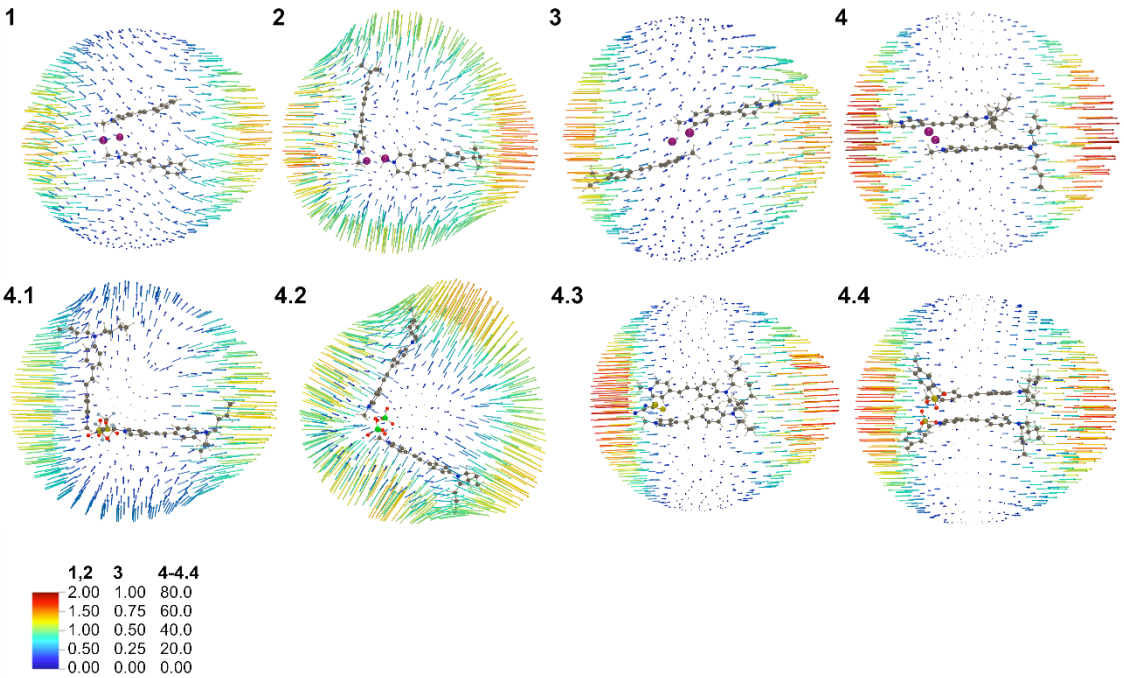

Figure 5. Unit sphere representation of the first hyperpolarizability for selected $(AC)_2$ dimers having a strong 1-D character. The values of 3 (**1**, **2**), 5 (**3**), and 1 (**4**-**4.4**) 10^{-4} Å a.u.$^{-1}$ were used to convert the induced dipole moment in Angstroms and the color maps are scaled by a factor of 10^{-3} a.u.

3.4. Excitation energies

Linear absorption spectra were simulated by employing the IEFPCM(chloroform)/TD-DFT/M06-2X/6-311+G(d) method for the 20 lowest-lying excited states. The spectrum of each complex is the average over the spectra of 100 configurations, each of them being obtained using 20 Lorentzian functions centered at the excitation energies and whose amplitude is proportional to the corresponding oscillator strength. The use of different full-

width at half-maximum values shows a small effect on the smoothness of the line-shape of the simulated spectra (**Figure S5**), so that, in **Figure 6**, a 0.4 eV value was adopted for each Lorentzian function. From these spectra, the λ_{max} values were defined as the λ value at maximum intensity (I_{max}). These values are collected in **Table 4** together with the ones corresponding to the parent AC complexes.

Increasing the strength of the donor substituent R in the stilbazolium cations (from **1** to **4**) induces a shift in λ_{max} from 340 to 436 nm together with an increase of intensities up to 24%. On the other hand, λ_{max} and I_{max} are much less sensitive to the nature of the anions. The absorption properties of the AC complexes are globally weakly impacted by aggregation effects. λ_{max} values are slightly blue-shifted upon aggregation, while intensity values before normalization slightly decrease when going from AC to $(AC)_2$ complexes. Indeed, for **1**, the $I_{max}(AC)_2$ / $2I_{max}(AC)$ ratio amounts to 0.94. The largest blue shift obtained for **4.4** is consistent with its preferential H-type aggregation, while the absorption spectra of preferential Λ-shape structures show very small variation owing to the weak interactions between the electron clouds of the stilbazolium cations.

Table 4. Theoretical and experimental linear absorption wavelengths (λ_{max}, nm), excitation energies (ΔE_{max}, eV), and normalized I_{max} intensities.[a]

Complex	λ_{max}, ΔE_{max}(calc.)	I_{max} (calc.)	λ_{max}, ΔE_{max}[b] (exp.)
1	340 (349), 3.65 (3.55)	1.00 (1.00)	340, 3.47
2	354 (356), 3.50 (3.48)	1.15 (1.08)	354, 3.29
3	431 (438), 2.88 (2.83)	1.23 (1.14)	431, 2.47
4	436 (445), 2.84 (2.79)	1.24 (1.21)	436, 2.39
4.1	435 (439), 2.85 (2.82)	1.28 (1.23)	435, 2.41
4.2	433 (438), 2.86 (2.83)	1.23 (1.23)	433, 2.38
4.3	433 (441), 2.86 (2.81)	1.22 (1.19)	433, 2.41
4.4	417 (431), 2.97 (2.88)	1.22 (1.20)	417, 2.44

[a] The values of the corresponding AC complexes are given in parentheses.[17]
[b] Values taken from Ref. 2.

The λ_{max} values computed for $(AC)_2$ dimers correlate well with the experimental data, although they are systematically underestimated by 0.2-0.5 eV, as generally observed for TD-DFT calculations using the M06-2X DFT functional.[40] Although the agreement could be improved by using another type of DFT functional such as one including long-range corrections, M06-2X was chosen owing to its good performance to evaluate nonlinear responses, and the same DFT functional has to be employed for linear and NLO properties

to describe frequency dispersion effects on possible resonances. In the present case, the transition wavelengths of all complexes are far from the 1907 nm excitation wavelength and its harmonic resonances, ensuring that the NLO responses are not contaminated by frequency dispersion effects. Moreover, **Figure 6** evidences that the UV/Vis absorption spectra can be determined in very good approximation by considering only two electronic excitations (S_{13}-S_{14} for **1** and S_1-S_2 for all other complexes) except for **2**, where many small contributions derive from several excitations to S_1-S_{12} states. Those excitations correspond to π- π^* transitions located on either of the cations.

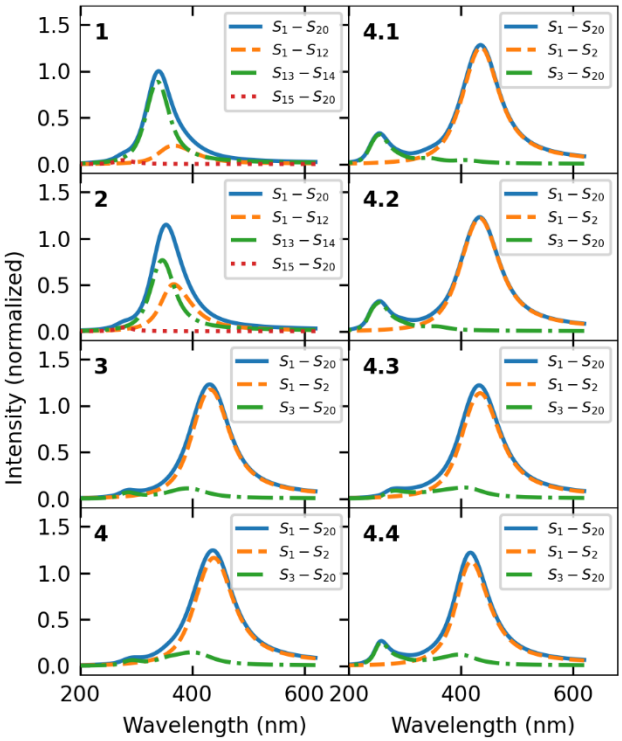

Figure 6. Simulated UV/Vis absorption spectra and contributions from dominant excited states, as obtained from the average over the spectra of 100 configurations issued from MD trajectories.

3.5. Structure-NLO properties relationships

In this section, we attempt to capture the relationships between different molecular properties and the NLO responses. Many types of functions can be used to model the data; however, the pair correlation plots (**Figure S6**) suggest absence or linear-like correlation and we, therefore, adopted the linear regression model to investigate the structure-NLO properties relationships. To facilitate the analyses, the Cartesian frame is defined such that the β vector is parallel to the x-axis. Therefore, $\mu\beta_{//}$ is directly proportional to the product between μ_x and β_x. The quality of the correlation in the linear regressions is characterized by the R^2 coefficients (**Figure 7**): if the R^2 value is close to 1 the model can be used as a

predictive tool. The absence of correlation between $\gamma_{//}$ and $\beta_{//}$ corroborates the fact that $\beta_{//}$ requires molecular asymmetry but not $\gamma_{//}$ as well as with the fact that the effects of dimerization are different on the second- and third-order responses. Then, moderate correlations are observed between $\beta_{//}$ and β_x with R^2 values in 0.55-0.88 range, with the exception of **1** (R^2 = 0.24). The partial relationship between $\beta_{//}$ and β_x originates from the fact that variations on $\beta_{//}$ are also dictated by μ_x, *i.e.* by the relative position of the anions with respect to the cations. This last statement is substantiated by the correlation between $\beta_{//}$ and $\cos(\theta_{(\mu,\beta)})$. For β_{HRS} versus $\beta_{//}$, similar correlations are found as for $\beta_{//}$ versus β_x while the correlation analyses demonstrate that β_{HRS} is mostly determined by β_x (R^2 values larger than 0.88).

A correlation is found between each of the three NLO responses ($\beta_{//}$, β_{HRS}, and $\gamma_{//}$) and θ_{CPLX} and, to a lower extent, with the r_{1x} and r_{2x}, which determine how the harmonophores are aligned along the x-axis. The correlation with θ_{CPLX} confirms that parallel stacking reinforces the responses or, in other words, that anti-parallel stacking is detrimental. This aspect is better evidenced for the second-order responses than for the third-order one because the former vanish for centrosymmetric systems. The absence of additional correlations between the NLO responses and geometric factors highlights the fact that they cannot be related to a single molecular descriptor but that they result from more complex inter-relationships implying simultaneously several variables. The R^2 coefficients for the three analyzed NLO responses ($\beta_{//}$, β_{HRS}, and $\gamma_{//}$) versus the geometric factors are presented in **Figure S7**.

For typical push-pull compounds with strong charge-transfer excitations, the simplest two-level model approximation can provide reasonable results for the NLO responses. In such approximation, the NLO responses are correlated to i) the oscillator strength (f), ii) the inverse-square of excitation energy ($1/\Delta E^2$), and iii) the change of dipole moment upon excitation. Such relationship was partially demonstrated for the parent AC complexes where reasonable linear correlation was observed for β_x *vs* ΔE^{-2} and f. However, the $(AC)_2$ dimers present two low-energy dipole-allowed excitations and the two-level approximation is reliable if only one of these excitations dictates the NLO responses.

Hence, the correlations between the β_{HRS} *vs* ΔE^{-2} and f were analyzed for each of these two excitations independently. The weak correlation (**Figure S8**) shows that the NLO responses is not dictated by only one excitation requiring more refined models to understand the relationships between the linear and nonlinear optical responses. Following the few-

state models, the three-level approximation could indicate any correlation. However, it includes extra contributions depending on the excited-excited transition dipole moment increasing substantially the complexity of such analyses. Yet, the fact that the UV/Vis spectra negligibly change upon the formation of $(AC)_2$ dimers combined with weak linear correlation observed between the linear and nonlinear responses argues that both AC complexes are scattering the light as a dimer and not as two independent AC monomers.

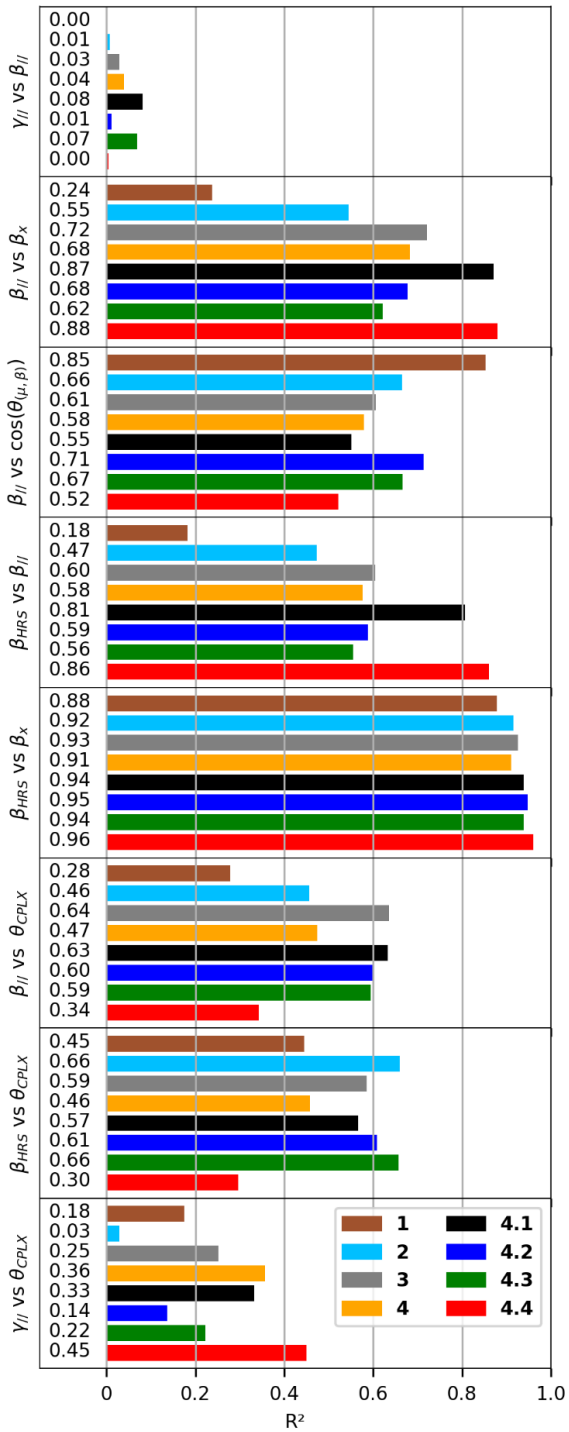

Figure 7. Linear correlation analyses between pairs of molecular properties. The nonlinear optical properties are represented by β_x, $\beta_{//}$, β_{HRS}, and $\gamma_{//}$. $\theta_{(\mu,\beta)}$ is the angle between the μ and β vectors. θ_{CPLX} represents the angle between the two cations.

3.6. Comparisons with Experiments

EFISHG experiments evidenced a large dependence of $\left[\mu\beta_{//}\right]_{eff}$ on the concentration.[2] The wide range of measured values originates from two different effects having opposite consequences: i) the aggregation of the AC pairs, which impacts the centrosymmetry of the complex and may either enhance or damp the second-order NLO responses, and ii) the dissociation of the AC pairs into solvated ions, which leads to spurious overestimations of the NLO responses.

Overall, the $\left[\mu\beta_{//}\right]_{eff}$ values computed for **1**-**4**, be they obtained for AC or $(AC)_2$ complexes, qualitatively reproduces the experimental trends, and evolve in the order **1** < **2** << **3** < **4**. However, whatever the concentration, the enhancement of the effective EFISHG responses observed experimentally for **3** and **4** is much smaller than that predicted by TDDFT calculations. Indeed, the NLO responses of **1** and **2** are better described by calculations carried out on single AC pairs, while **3** and **4** are conversely better described when considering $(AC)_2$ dimers. Selecting the corresponding values, the relative $\left[\mu\beta_{//}\right]_{eff}$ values computed for the **1**-**4** series are: **1** (1.0), **2** (2.0), **3** (5.6) and **4** (6.8), which shows a good agreement with experimental data measured for highly concentrated solutions: **1** (1.0), **2** (1.2), **3** (5.9) and **4** (6.4).

Comparisons between theoretical and experimental results are more delicate for complexes implying different anions. Experimentally, **4.1** and **4.2** exhibit the largest dependence of their effective EFISHG response on the concentration, with relative $\left[\mu\beta_{//}\right]_{eff}$ values decreasing as 1.0; 0.6; 0.2 (**4.1**) and 1.0; 0.6; 0.1 (**4.2**) for concentrations of 1 10^{-4}, 5 10^{-4}, and 1 10^{-3} M. In both **4.1** and **4.2**, calculations predict a decrease by half of the EFISHG response upon aggregation of AC pairs into $(AC)_2$ dimers, which is consistent with the experimental results measured for the two lowest concentrations. These results suggest that only single AC pairs are present at 1 10^{-4} M, while $(AC)_2$ dimers are the most representative species at 5 10^{-4} M. The decrease of the EFISHG responses of these two complexes as the concentration further increases suggests that larger aggregates are formed, which was also observed in the first step of high-concentration MD simulations.

A different behavior is observed for **4.4**, which shows a weaker lowering and a saturation of the relative $\left[\mu\beta_{//}\right]_{eff}$ values with increasing concentrations (1.0; 0.7; 0.6). This result is also consistent with TD-DFT calculations, which predict a smaller decrease of the EFISHG response (of 0.9) when going from AC to $(AC)_2$ complexes. The saturation observed for this

species suggests that no larger complexes than dimers are formed upon further increasing the concentration, which might be ascribed to the propension of this complex to form H aggregates. Finally, no concentration effects are observed for **4.3**. Therefore, since the theoretical calculations also predict a decrease of the relative $[\mu\beta_{//}]_{eff}$ values with aggregation, it is suggested that only single AC complexes are present in the measurements.

4. Conclusions

This theoretical study committed to unraveling the EFISHG responses on aggregates of anion-cation complexes, by using a sequential approach combining molecular dynamics and DFT calculations. The complexes considered showed a strong self-aggregation behavior in MD simulations within high-concentration conditions and formed stable dimer aggregates, $(AC)_2$, which can adopt different structural shapes from stacked, Λ-, to head-to-head configurations. These various structures are associated with different symmetries, which impact their NLO responses. Although our results corroborate the commonly admitted fact that the second-order contribution dominates the global EFISHG response, the aggregation effects provided distinct trends on $\mu\beta_{//}$ and $\gamma_{//}$. While the $\mu\beta_{//}$ responses of dimers are about half that computed for the parent AC pairs, the $\gamma_{//}$ are reduced by only 10%. These these distinct trends are ascribed to the formation of dimers adopting mainly Λ- and head-to-head shapes, increasing the centrosymmetric character, in comparison to the monomers, a situation in which the second-order response cancels out. Moreover, like $\gamma_{//}$, the UV/Vis absorption spectra are also weakly impacted by the formation of $(AC)_2$ dimers. The presence of strong amino donor groups in the cation enhances the $\mu\beta_{//}$ response by one order of magnitude and $\gamma_{//}$ by about a factor of 2. As observed for the AC pairs, the dipole moment orientation plays an important role in tuning the $\beta_{//}$ response, which is associated with the relative position of the anions with respect to the cations. Moreover, in the case of the HRS response, calculations have evidenced (i) similar effects of dimeric aggregations to those on $\mu\beta_{//}$ and (ii) the vanishing of the 1-D-like symmetry character of the β_{HRS} responses of the $(AC)_2$ dimers with respect to the parent AC pairs.

Consolidating the EFISHG results of this work with the values previously obtained for single AC pairs,[17] we have related the theoretical-experimental values as follows: (i) complexes **1** and **2** are better described by AC monomers while **3** and **4** by $(AC)_2$ dimers; (ii) this

agreement is observed with the measurements performed at highly concentrated solutions (1 10^{-3} M) while at lower concentrations, the $\mu\beta_{//}$ response increases, figuring out the dissociation of the ion pairs; (iii) for complexes **4.1** and **4.2**, owing to the variations of the $\mu\beta_{//}$ response as a function of the concentration, single AC pairs are present at a concentration of 1 10^{-4} M while at 5 10^{-4} M, $(AC)_2$ dimers are the dominating species; (iv) only single AC complexes are present in the measurements carried out at the different concentrations on **4.3**, which is the only system where the $\mu\beta_{//}$ response is not concentration-dependent; and (v) complex **4.4** showed the smallest decrease of the theoretical EFISHG response due to dimerization, which is consistent with the measurements and which suggests that no larger complexes than dimers are formed even at high concentration.

This work constitutes a step forward for the modeling of the NLO responses of complexes in solution. Still, in general, AC complexes might form aggregates larger than dimers, so that other studies could go beyond the dimers and consider trimers, tetramers, etc. Yet, the current study has highlighted the relationship between the variations of hyperpolarizabilities and the shape of the dimer. Though the model adopted here performed well, as a perspective with respect to the level of approximation, it would be interesting to investigate approaches where the effects of the surrounding are described in TD-DFT calculations by using a structured or explicit environment, using an electrostatic discrete local field approach, as it was recently demonstrated.[41] Finally, this work also demonstrated that the intramolecular descriptors related to π-conjugation within the cations are not linearly correlated to the NLO responses, which might call for the development of new computational approaches such as machine learning[42] to unravel the interplay between structural parameters and NLO properties.

Associated Content

Supporting Information

Integration grid effects on the NLO properties, initial geometries of the $(AC)_2$ dimers for MD simulations in chloroform, cumulative averages of the NLO properties and their respective standard deviations, UV/Vis spectra for different line-width values, pair correlation plots, and linear correlation analyses for optical versus geometrical properties.

Author Information

Corresponding Author

* E-mail: benoit.champagne@unamur.be

ORCID

Tárcius N. Ramos: 0000-0002-5806-6796
Benoît Champagne: 0000-0003-3678-8875
Frédéric Castet: 0000-0002-6622-2402

Notes

The authors declare no competing financial interest.

Acknowledgments

TR thanks the Fonds Spécial de Recherche of UNamur for his postdoctoral grant. The calculations were performed on the computers of the « Consortium des Équipements de Calcul Intensif (CÉCI) » (http://www.ceci-hpc.be), including those of the « UNamur Technological Platform of High-Performance Computing (PTCI) » (http://www.ptci.unamur.be), for which we gratefully acknowledge the financial support from the FNRS-FRFC, the Walloon Region, and the University of Namur (Conventions No. 2.5020.11, GEQ U.G006.15, U.G018.19, 1610468, and RW/GEQ2016) as well as on Zenobe, the Tier-1 facility of the Walloon Region (Convention 1117545).

5. References

(1) Alain, V.; Blanchard-Desce, M.; Ledoux-Rak, I.; Zyss, J. Amphiphilic Polyenic Push–Pull Chromophores for Nonlinear Optical Applications. *Chem. Commun.* **2000**, *6*, 353–354.

(2) Tessore, F.; Cariati, E.; Cariati, F.; Roberto, D.; Ugo, R.; Mussini, P.; Zuccaccia, C.; Macchioni, A. The Role of Ion Pairs in the Second-Order NLO Response of 4-X-1-Methylpiridinium Salts. *ChemPhysChem* **2010**, *11*, 495–507.

(3) Cariati, E.; Dragonetti, C.; Lucenti, E.; Nisic, F.; Righetto, S.; Roberto, D.; Tordin, E. An Acido-Triggered Reversible Luminescent and Nonlinear Optical Switch Based on a Substituted Styrylpyridine: EFISH Measurements as an Unusual Method to Reveal a Protonation–Deprotonation NLO Contrast. *Chem. Commun.* **2014**, *50*, 1608–1610.

(4) Pielak, K.; Tonnelé, C.; Sanguinet, L.; Cariati, E.; Righetto, S.; Muccioli, L.; Castet, F.; Champagne, B. Dynamical Behavior and Second Harmonic Generation Responses in Acido-Triggered Molecular Switches. *J. Phys. Chem. C* **2018**, *122*, 26160–26168.

(5) Tessore, F.; Locatelli, D.; Righetto, S.; Roberto, D.; Ugo, R.; Mussini, P. An Investigation on the Role of the Nature of Sulfonate Ancillary Ligands on the Strength and Concentration Dependence of the Second-Order NLO Responses in $CHCl_3$ of Zn(II) Complexes with 4,4'-trans-$NC_5H_4CH{=}CHC_6H_4NMe_2$ and 4,4'-trans,trans-$NC_5H_4(CH{=}CH)_2C_6H_4NMe_2$. *Inorg. Chem.* **2005**, *44*, 2437–2442.

(6) Pizzotti, M.; Tessore, F.; Biroli, A. O.; Ugo, R.; Angelis, F. De; Fantacci, S.;

Sgamellotti, A.; Zuccaccia, D.; Macchioni, A. An EFISH, Theoretical, and PGSE NMR Investigation on the Relevant Role of Aggregation on the Second Order Response in $CHCl_3$ of the Push−Pull Chromophores [5-[[4'-(dimethylamino)phenyl]ethynyl]-15-[(4''-nitrophenyl)ethynyl]-10,20-diphenylporphyrinate] M(II) (M=Zn, Ni). *J. Phys. Chem. C* **2009**, *113*, 11131–11141.

(7) Di Bella, S.; Ratner, M. A.; Marks, T. J. Design of Chromophoric Molecular Assemblies with Large Second-Order Optical Nonlinearities. A Theoretical Analysis of the Role of Intermolecular Interactions. *J. Am. Chem. Soc.* **1992**, *114*, 5842–5849.

(8) Maroulis, G. Static Hyperpolarizability of the Water Dimer and the Interaction Hyperpolarizability of Two Water Molecules. *J. Chem. Phys.* **2000**, *113*, 1813–1820.

(9) Castet, F.; Champagne, B. Simple Scheme to Evaluate Crystal Nonlinear Susceptibilities: Semiempirical AM1 Model Investigation of 3-Methyl-4-Nitroaniline Crystal. *J. Phys. Chem. A* **2001**, *105*, 1366–1370.

(10) Wang, B.-Q.; Li, Z.-R.; Wu, D.; Hao, X.-Y.; Li, R.-J.; Sun, C.-C. Ab Initio Study of the Interaction Hyperpolarizabilities of H-Bond Dimers between Two π-Systems. *J. Phys. Chem. A* **2004**, *108*, 2464–2468.

(11) Nakano, M.; Takebe, A.; Kishi, R.; Fukui, H.; Minami, T.; Kubota, K.; Takahashi, H.; Kubo, T.; Kamada, K.; Ohta, K.; et al. Intermolecular Interaction Effects on the Second Hyperpolarizability of Open-Shell Singlet Diphenalenyl Radical Dimer. *Chem. Phys. Lett.* **2008**, *454*, 97–104.

(12) Suponitsky, K. Y.; Masunov, A. E. Supramolecular Step in Design of Nonlinear Optical Materials: Effect of π…π Stacking Aggregation on Hyperpolarizability. *J. Chem. Phys.* **2013**, *139*, 094310.

(13) Fominykh, O. D.; Sharipova, A. V.; Yu. Balakina, M. The Choice of Appropriate Density Functional for the Calculation of Static First Hyperpolarizability of Azochromophores and Stacking Dimers. *Int. J. Quantum Chem.* **2016**, *116*, 103–112.

(14) Wang, L.; Ye, J.-T.; Wang, H.-Q.; Xie, H.-M.; Qiu, Y.-Q. Self-Assembled Donor–Acceptor Chromophores: Evident Layer Effect on the First Hyperpolarizability and Two-Dimensional Charge Transfer Character. *J. Phys. Chem. C* **2017**, *121*, 21616–21626.

(15) Zaleśny, R.; Medved', M.; Góra, R. W.; Reis, H.; Luis, J. M. Partitioning of Interaction-Induced Nonlinear Optical Properties of Molecular Complexes. I. Hydrogen-Bonded Systems. *Phys. Chem. Chem. Phys.* **2018**, *20*, 19841–19849.

(16) Böttcher, C. J. F. *Theory of Electric Polarization*, Second Edi.; Elsevier: Amsterdam, 1973.

(17) Ramos, T. N.; Canuto, S.; Champagne, B. Unraveling the Electric Field-Induced Second Harmonic Generation Responses of Stilbazolium Ion Pairs Complexes in Solution Using a Multiscale Simulation Method. *J. Chem. Inf. Model.* **2020**, *60*, 4817–4826.

(18) Mennucci, B.; Cammi, R.; Tomasi, J. Medium Effects on the Properties of Chemical Systems: Electric and Magnetic Response of Donor-Acceptor Systems within the Polarizable Continuum Model. *Int. J. Quantum Chem.* **1999**, *75*, 767–781.

(19) Tomasi, J.; Mennucci, B.; Cammi, R. Quantum Mechanical Continuum Solvation Models. *Chem. Rev.* **2005**, *105*, 2999–3094.

(20) Coutinho, K.; Canuto, S. Solvent Effects from a Sequential Monte Carlo - Quantum Mechanical Approach. *Adv. Quantum Chem.* **1997**, *28*, 89–105.

(21) Coutinho, K.; Canuto, S.; Zerner, M. C. Monte Carlo-Quantum Mechanics Study of

the Solvatochromic Shifts of the Lowest Transition of Benzene. *J. Chem. Phys.* **2000**, *112*, 9874–9880.

(22) Verbiest, T.; Clays, K.; Rodriguez, V. *Second-Order Nonlinear Optical Characterization Techniques*; CRC Press: New York, 2009.

(23) Ledoux, I.; Zyss, J. Influence of the Molecular Environment in Solution Measurements of the Second-Order Optical Susceptibility for Urea and Derivatives. *Chem. Phys.* **1982**, *73*, 203–213.

(24) Levine, B. F.; Bethea, C. G. Second and Third Order Hyperpolarizabilities of Organic Molecules. *J. Chem. Phys.* **1975**, *63*, 2666–2682.

(25) Willetts, A.; Rice, J. E.; Burland, D. M.; Shelton, D. P. Problems in the Comparison of Theoretical and Experimental Hyperpolarizabilities. *J. Chem. Phys.* **1992**, *97*, 7590.

(26) Hendrickx, E.; Clays, K.; Persoons, A. Hyper-Rayleigh Scattering in Isotropic Solution. *Acc. Chem. Res.* **1998**, *31*, 675–683.

(27) Hockney, R. W.; Goel, S. P.; Eastwood, J. W. Quiet High-Resolution Computer Models of a Plasma. *J. Comput. Phys.* **1974**, *14*, 148–158.

(28) Berendsen, H. J. C.; Postma, J. P. M.; van Gunsteren, W. F.; DiNola, A.; Haak, J. R. Molecular Dynamics with Coupling to an External Bath. *J. Chem. Phys.* **1984**, *81*, 3684–3690.

(29) Bussi, G.; Donadio, D.; Parrinello, M. Canonical Sampling through Velocity Rescaling. *J. Chem. Phys.* **2007**, *126*, 014101.

(30) Essmann, U.; Perera, L.; Berkowitz, M. L.; Darden, T.; Lee, H.; Pedersen, L. G. A Smooth Particle Mesh Ewald Method. *J. Chem. Phys.* **1995**, *103*, 8577–8593.

(31) Jorgensen, W. L.; Maxwell, D. S.; Tirado-Rives, J. Development and Testing of the OPLS All-Atom Force Field on Conformational Energetics and Properties of Organic Liquids. *J. Am. Chem. Soc.* **1996**, *118*, 11225–11236.

(32) Breneman, C. M.; Wiberg, K. B. Determining Atom-Centered Monopoles from Molecular Electrostatic Potentials. The Need for High Sampling Density in Formamide Conformational Analysis. *J. Comput. Chem.* **1990**, *11*, 361–373.

(33) McDonald, N. A.; Carlson, H. A.; Jorgensen, W. L. Free Energies of Solvation in Chloroform and Water from a Linear Response Approach. *J. Phys. Org. Chem.* **1997**, *10*, 563–576.

(34) van Der Spoel, D.; Lindahl, E.; Hess, B.; Groenhof, G.; Mark, A. E.; Berendsen, H. J. C. GROMACS: Fast, Flexible, and Free. *J. Comput. Chem.* **2005**, *26*, 1701–1718.

(35) Berendsen, H. J. C.; van der Spoel, D.; van Drunen, R. GROMACS: A Message-Passing Parallel Molecular Dynamics Implementation. *Comput. Phys. Commun.* **1995**, *91*, 43–56.

(36) Zhao, Y.; Truhlar, D. G. The M06 Suite of Density Functionals for Main Group Thermochemistry, Thermochemical Kinetics, Noncovalent Interactions, Excited States, and Transition Elements: Two New Functionals and Systematic Testing of Four M06-Class Functionals and 12 Other Function. *Theor. Chem. Acc.* **2008**, *120*, 215–241.

(37) Lescos, L.; Sitkiewicz, S. P.; Beaujean, P.; Blanchard-Desce, M.; Champagne, B.; Matito, E.; Castet, F. Performance of DFT Functionals for Calculating the Second-Order Nonlinear Optical Properties of Dipolar Merocyanines. *Phys. Chem. Chem. Phys.* **2020**, *22*, 16579–16594.

(38) Castet, F.; Bogdan, E.; Plaquet, A.; Ducasse, L.; Champagne, B.; Rodriguez, V. Reference Molecules for Nonlinear Optics: A Joint Experimental and Theoretical

Investigation. *J. Chem. Phys.* **2012**, *136*, 024506.

(39) Frisch, M. J.; Trucks, G. W.; Schlegel, H. B.; Scuseria, G. E.; Robb, M. A.; Cheeseman, J. R.; Scalmani, G.; Barone, V.; Petersson, G. A.; Nakatsuji, H.; et al. *Gaussian16,* revision A03. Gaussian, Inc.: Wallingford CT, **2016**.

(40) Laurent, A. D.; Jacquemin, D. TD-DFT Benchmarks: A Review. *Int. J. Quantum Chem.* **2013**, *113*, 2019–2039.

(41) Hrivnák, T.; Reis, H.; Neogrády, P.; Zaleśny, R.; Medved', M. Accurate Nonlinear Optical Properties of Solvated para-Nitroaniline Predicted by an Electrostatic Discrete Local Field Approach. *J. Phys. Chem. B* **2020**, *124*, 10195–10209.

(42) Tuan-Anh, T.; Zaleśny, R. Predictions of High-Order Electric Properties of Molecules: Can We Benefit from Machine Learning? *ACS Omega* **2020**, *5*, 5318–5325.